Optical coherence tomography imaging of plant root growth in soil

Curtis J. Larimer, Elizabeth H. Denis, Jonathan D. Suter, James J. Moran

Complex interactions between roots and soil provide the nutrients and physical support required for robust plant growth. Yet, visualizing the root–soil interface is challenged by soil's opaque scattering characteristics. Herein, we describe methods for using optical coherence tomography (OCT) to provide non-destructive 3D and cross-sectional root imaging not available with traditional bright-field microscopy. OCT is regularly used for bioimaging, especially in ophthalmology, where it can detect retinal abnormalities. Prior use of OCT in plant biol-ogy has focused on surface defects of above-ground tissues, predominantly in food crops. Our results show OCT is also viable for detailed, *in situ* study of living plant roots. Using OCT for direct observations of root growth in soil can help elucidate key interactions between root morphology and various components of the soil environment including soil structure, microbial communities, and nutrient patches. Better understanding of these interactions can guide efforts to improve plant nutrient acquisition from soil to increase agricultural efficiency as well as better understand drivers of plant growth in natural systems.

1. INTRODUCTION

Soil is highly heterogeneous due to interacting geochemical, biological, and physical processes, which can create strong nutrient gradients at pore-sized (roughly millimeter, mm) or smaller scales [1]. Roots must navigate this complex environment to efficiently e xtract n eeded n utrients t o s upport p lant growth. Previous work has demonstrated morphological adaptation of roots, highlighted by larger rates of root branching to focus plant investment in regions of soil with higher nutritional value to the plant [2]. Other work demonstrates a link between the formation of root hairs and a plant's interaction with and ability to harvest nutrients from soil [3]. Additionally, a suite of nutrient exchange processes can be facilitated by symbiotic interactions between plant roots and fungi, which effectively extend the spatial reach of nutrient collection from soil well beyond the root boundary itself [4,5]. Examining the complex coordination of these nutrient acquisition strategies is crucial to establishing a holistic understanding of nutrient exchange between soil and plants and may form a foundation for enriching these processes to improve agricultural or natural plant growth [6]. Each of the above processes can be visually observed (with magnification), but high-throughput tools for detailed, three-dimensional tracking of these physical interactions during root growth are largely lacking.

The principal challenge is that soil itself can obscure *in situ* root system visualization. To avoid this issue, plants are sometimes grown in liquid culture, surfaces of agar or paper, or in transparent gel growth media that can enable visualization but may not be representative of the 3D nature of growth in the natural environments (i.e., soil) and may restrict analysis of larger plants [7–10]. Imaging techniques such as x-ray micro-focus computed tomography (x-ray μCT) and synchrotron tomography (SR-CT) can enable imaging directly within soil, but both have limitations. X-ray μCT functions on the nanometer (nm) to decimeter (dm) scale but has limited sample throughput, and the resulting long scan times can negatively impact soil biota and are thus not truly non-destructive to the holistic root–soil system [9]. Synchrotron tomography [nm to centimeter (cm) scale], is limited by sample size, throughput, expense, and accessibility, and it is not transportable to the field [10,11].

Optical coherence tomography (OCT), often described as an "optical ultrasound," offers a potential solution for non-destructive imaging and tomography of roots. OCT is a commonly applied technique for studying the morphology

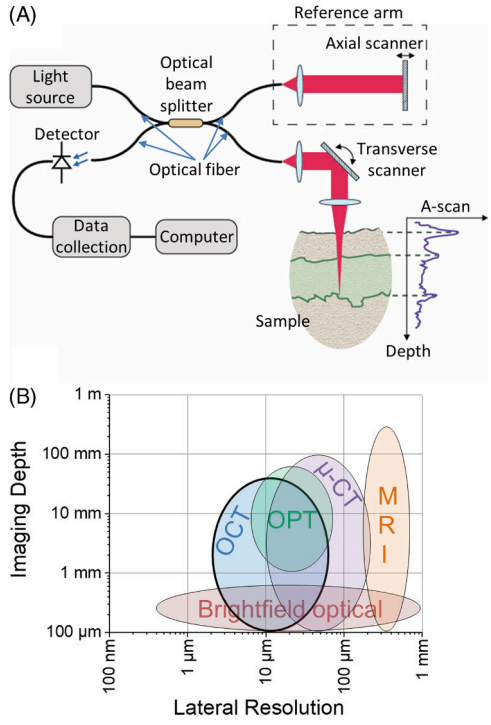

Fig. 1. (A) Major components and functions of an optical coherence tomography (OCT) imaging system are laid out as a Michelson interferometer. Light from a broadband source is split by an optical beam splitter and sent to both a reference arm and sample arm. Recombined light creates interference that is observed at a photodetector. Raw spectra are converted to 3D images. (B) OCT has a combination of lateral resolution and imaging depth that is not available with other root imaging methods (e.g., optical projection tomography [OPT] [25,26], micro-computed tomography [µ-CT] [27,28], magnetic resonance imaging [MRI] [29], and bright-field optical microscopy).

and changes in human skin [12], retina [13], veins and arteries, and other soft tissues [14,15]. Functionally, OCT uses interferometry to record the optical path of photons reflected from the layers of soft tissues. A near-infrared laser light source scans over the surface of a sample to produce depth-resolved cross sections, which can be assembled into a full 3D tomogram. Figure 1(A) shows the major optical components of an OCT system.

OCT imaging systems can achieve spatial resolution of approximately 2–4 µm (lateral resolution is restricted by the optical diffraction limit and lateral sampling rate, while the axial resolution is inversely proportional to the bandwidth of the light source), and depths of up to 10 mm can be resolved [14,16], which gives it a unique combination of lateral resolution and imaging depth when compared to other root imaging techniques [as shown in Fig. 1(B)]. OCT imaging is also relatively fast (scans can take from 10 s to 5 min depending on settings) and non-destructive (the laser light source is relatively low power). In terms of plant biology, OCT has been demonstrated for imaging of subsurface layers of fruits, seeds, and plant leaves [17–20], stomata [21], and leaf defects that result from the stresses associated with environmental pollutants [22], drought [23], and disease [24]. Despite this previous work, OCT has not been used to study root systems in soil, likely owing to the difficulty of imaging in a highly scattering medium.

In this paper, we describe application of OCT imaging to the study of roots, including those grown in soil. First, we present a traditional use of OCT to monitor the emergence of roots from germinating seeds through air. Then we describe the custom growing and imaging conditions that are needed to achieve high-quality images in the challenging soil medium. As OCT imaging is non-destructive, roots were imaged at regular intervals while growing through soil, and the resulting series of images enabled estimation of the growth rate of the root tip and several root hairs. In the future, we envision continued use of these methods to better understand root systems and their interaction with the soil and symbiotic species such as fungi and bacteria.

2. METHODS

A. Plants, Soil, and Growth Conditions

Seeds (*Panicum virgatum* L., PI 469228, switchgrass, variety Cave-in-Rock, provided from the USDA National Plant Germplasm System) were germinated on a layer of wet Kimwipes in a petri dish. Images were collected from germinating seeds every 3 h for several days in order to capture the time at which roots emerged. A subset of the germinated seedlings were planted in rhizoboxes (black high-density polyethylene, 15 cm × 20 cm × 1 cm) filled with soil (4 mm sieved) from the Kellogg Biological Station, Michigan, USA [Fig. 2(A)]. Rhizoboxes were placed in a Conviron walk-in growth chamber at an approximately 45 deg angle relative to horizontal to encourage root growth along a side transparent panel to optimize imaging of the root. Climate controlled conditions were 16 h of light at 22°C and 60% relative humidity and 8 hrs of dark at 18°C and 50% relative humidity. The plant grew in the chamber for 21 days. The side section of the rhizobox was removed and replaced with a transparent plexiglass panel. Sections of this clear panel not targeted for imaging were covered in aluminum foil to protect the soil and roots from ambient light exposure.

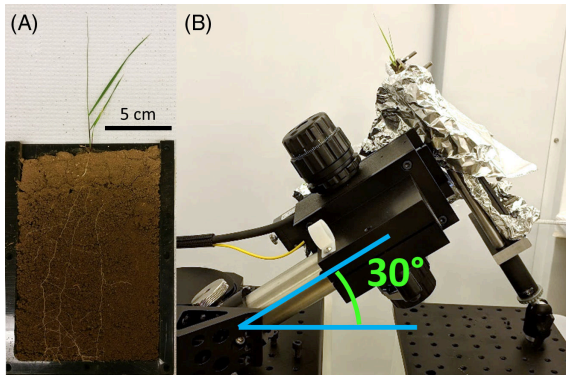

Fig. 2. (A) Photo of a switchgrass plant grown in a rhizobox. (B) Photo of the imaging setup showing the imaging end of the OCT system pointing up to the right at an angle of approximately 30° above horizontal. The imager sits ~3 mm from the surface of the rhizobox, which is covered in aluminum foil to block light from reaching roots during the experiment.

B. OCT Imaging Setup

Imaging was performed with a spectral domain OCT instrument system (Ganymede Model 210C1, ThorLabs, Newton, NJ). The laser light source has a center wavelength of 930 nm and was scanned at 36 kHz. A scanning lens (model OCT-LK3-BB) with ~25 mm working distance, 8 μm lateral resolution, and 2.9 μm axial resolution was used. Maximal scanning areas of 10 mm by 10 mm were explored, but we generally used smaller areas of between 2 to 7 mm lateral distance to minimize scanning time and resulting file sizes. ThorLabs ThorImage OCT 4.4 software was used to collect and process raw data into 3D tomograms. The software performs a fast Fourier transform of the raw spectral data and then takes the absolute value of the complex data to produce A-scans (i.e., the image intensity of each axial column in the field of view). For processing, three A-scans were averaged, and spectral shaping was applied. The averaged A-scan data for the full field were stored in decibels (dB), which was computed by taking the base-10 logarithm and multiplying by 20. A Hann apodization window was chosen to reduce imaging artifacts, and quadratic dispersion compensation was applied to reduce axial blurring. A grayscale color map was applied to the dB values of the 3D image using a dynamic range that was selected to filter out speckle in the air around samples.

Typically, OCT imaging systems are set up like traditional microscopes, with the imaging lens pointing down at a sample. However, as described above, plants were grown in rhizoboxes [see Fig. 2(A)] placed at an angle to encourage growth of the root against the transparent panel on one side of the box. For this research, a custom stand was built to accommodate imaging at adjustable angles, including pointing up at approximately 30° relative to horizontal [as shown in Fig. 2(B)]. The angle and pitch of the rhizobox was also made adjustable using a ball joint to facilitate aligning the sample perpendicular to the imager. Suitable imaging areas of seeds and roots were selected, and the imaging system was focused. A single imaging scan typically took 30–120 s to acquire, depending on the size of the field of view.

Time series image collection was enabled by using built-in scheduling features of the ThorImage software, and our applied collection intervals ranged from 15 min to 3 h for periods up to 6 days. The software was typically set to automatically collect data for 24–48 h, after which time we would archive collected data and reset the system for continued data collection. In several cases (especially for germinating seeds), images were collected over several days before roots began to emerge. Data that was collected was periodically moved to an external storage device to avoid exhausting the memory of the computer system. Image focus was adjusted as necessary at the start of each series of data collection.

Imaging roots and soil in proximity to a transparent panel resulted in a bright plane artifact in each image. Reflections of this plane above or below the primary root imaging data were eliminated by choosing a panel with thickness (approximately 3 mm) greater than the imaging depth. Using a thinner panel would result in multiple planar artifacts that could not easily be filtered because they would overlap the data of interest. The bright plane was removed using the clipping feature of the ThorImage software. As much as possible, identical clip settings were used for all images in a time series. Subtle shifts in the sample relative to the imager occasionally resulted in a change in the location of the viewing window in the image. Clipping was adjusted to accommodate these shifts. Images were exported from the ThorImage software as jpg images. Clipping was also used to generate cross sections, such as in Figs. 3 and 8.

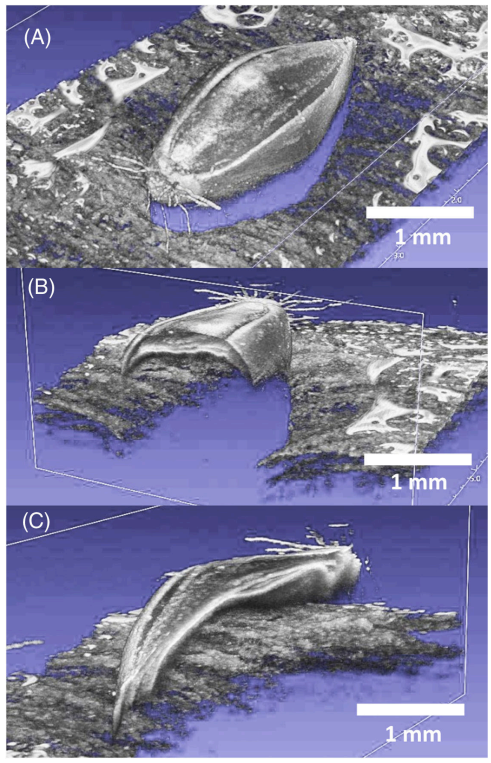

Fig. 3. (A) OCT image of a switchgrass seed on a wet paper towel at the time of root emergence. Cross sections of the image shown in A across the (B) width of the seed and the (C) length of the seed show the depth imaging capability. Scales are indicated by the bar in each image.

Exported images were subsequently processed using Adobe Photoshop CC 2019. Brightness and contrast were adjusted uniformly for all images in Figs. 3, 4, and 8(B) and 8(C). Visualizations of the time series were also created using this software. Visualization 1, Visualization 2, Visualization 3, Visualization 4, Visualization 5, and Visualization 6 were made from animated files exported from the ThorImage software.

The Tracker Video Analysis and Modeling tool, an open source software (available at physlets.org/tracker), was used to track the movement of a main root tip and two root hairs growing through soil. The software takes a video of the time series as input. The location of the tip of the root was selected manually by advancing the video "frame-by-frame" through each image in the time series. The distance the tip moved between images was automatically calculated by entering the image's scale. The Tracker software then used these distances and the time elapsed between images to calculate growth rate in millimeters per hour (mm/hr). The path that the root tip followed was also tracked to create a trace of movement. Data were plotted, and trend analysis was performed using graphing and analysis software (Origin 2019a).

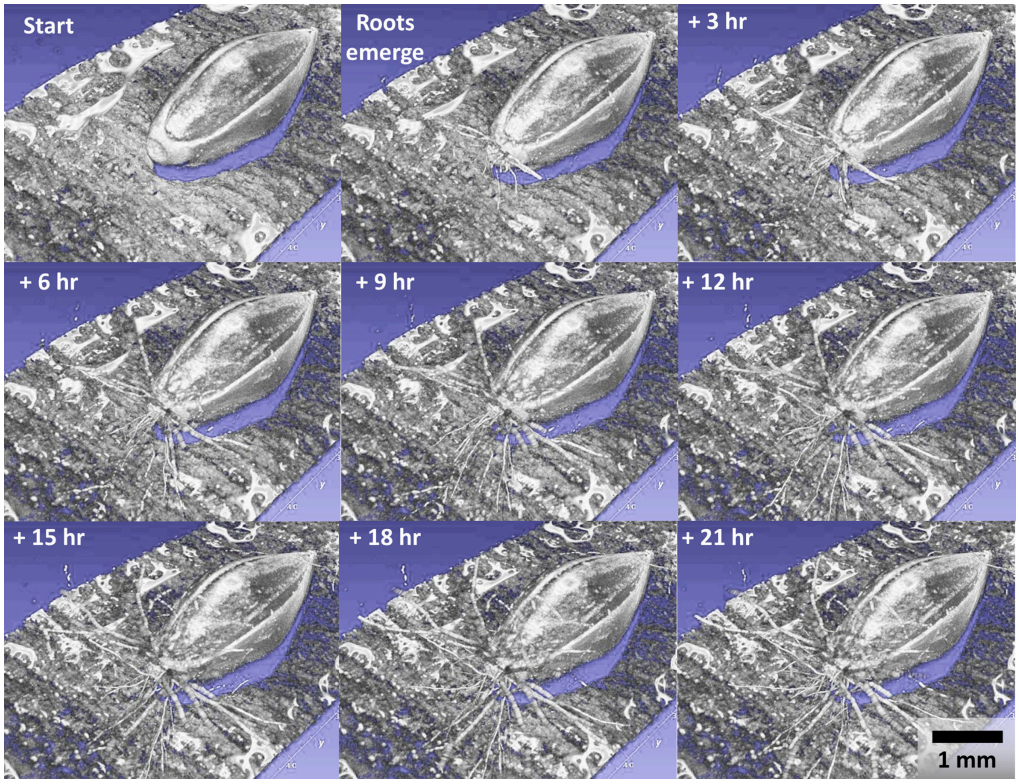

Fig. 4. Time series of OCT images of a switchgrass seed show the emergence of roots over 21 hrs. Scale is indicated by the bar in the lower right image.

3. RESULTS AND DISCUSSION

The first objective of this research was to ascertain the degree to which OCT could resolve the fine details of root structures and to establish procedures needed to perform time series imaging of roots within soil. We germinated switchgrass seeds on a wet paper towel to encourage germination while allowing for unobscured sample imaging. The seed was imaged every 3 hrs to enable tracking of root emergence and elongation from the seed. Figure 3 shows 3D images of the seed at the first time point after roots appeared (see also Visualization 1, which shows a rotating view of the same data), and the complementary horizontal and lengthwise cross-section images reveal some internal structures in the seed. The images clearly show fine roots emerging from the seed and branching out into the surrounding medium. The "shadow" effect visible under the seed in this image highlights one potential limitation of OCT, in that the method prevents collection of data from the surface under the seed because light cannot pass through the seed to reach structures underneath. Some artifacts of water in the paper towel are also visible around the seed. The presence of water in and around plant roots may influence OCT imaging because water can create a reflective surface and can also absorb near-IR light.

Figure 4 and Visualization 2 show time series of root growth from a germinating seed over time, which helps highlight the non-destructive nature of OCT. The panels of Fig. 4 show the first 21 hrs of a 39 hr observation period. The images clearly show lengthening and thickening of nascent roots, which radiate from the seed tip. Near the end of the observational window, many of the roots extend beyond the focal plane of the imaging system, leading to image blurring and other artifacts. This blurring highlights the need to ensure the sample is within suitable imaging boundaries to ensure the efficacy of quantitative measurements (e.g., root diameter), because root dimensions may appear to vary with the level of blurring.

Results of a separate experiment where two seeds were placed next to each other are shown in Visualization 3. The observation period was 69 h. Interestingly, this set of images also shows emergence of the thicker primary root in addition to a large collection of fine root hairs. The time series also shows one of the seeds being lifted towards the top of the imaging field near the end of the experiment. These experiments show it is possible to observe root growth over extended time periods (>72 h) using OCT.

After completing simple experiments with germinating seeds, we attempted imaging of roots in soil. Two conditions were created to enable imaging in this challenging medium. First, the roots were grown in an angled rhizobox, which encouraged growth in contact with a transparent imaging window. This would allow direct imaging of the root with a surrounding matrix of soil. Second, the imaging window was thick enough to avoid reflective artifacts in the depth region that was most of interest. Figure 5 shows an angled perspective of a switchgrass root growing in soil and a cross section of the root as it enters the field of view. Black arrows indicate the direction of root growth, and a series of hourly images (Fig. 6) shows the progression of root growth over 9 h. Visualization 4 shows the same growth with images every 15 min. The series clearly show the root pushing through the soil. Closer inspection (clearly seen in

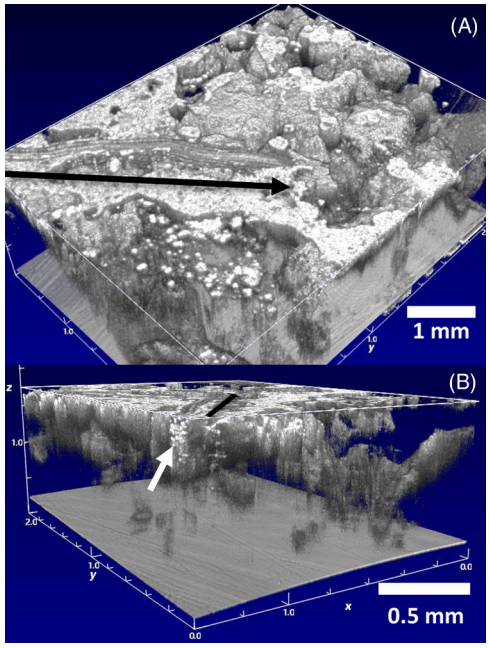

Fig. 5. OCT image of a switchgrass root in soil shown (A) from above and (B) from the side. The black arrow in A indicates the direction of growth of the root, which is directly above the arrow. The white arrow in B shows where the root is cross-sectioned at the edge of image.

Visualization 4) also reveals the emergence of root hairs from the sides of the main root. Visualization 5 shows images taken in a separate experiment over a time period of 44 hrs. Both sets of images show that OCT can be used to observe root growth in soil.

The images shown in Fig. 6 and Visualization 4 were further analyzed using tracker software to measure root growth rate, and the results are shown in Fig. 7. The growth rates of the primary root and two root hairs were measured by tracing the movement of the tips through the series of images. Figure 7 shows a trace of the path that the root tip follows overlaid on one of the images in the middle of the observed period. The root does not grow in a straight line as seen by the black trace in Fig. 7(B) and appears to be influenced by obstruction by soil mineral particulates. One period between 5 and 8 hrs in Visualization 4 shows the root pushing particulate material out of its path; the root changes direction and moves the particulate out of the way as it grows. Growth rate ranged from 0.02 to 0.15 mm/hr, which is of a similar order (a fraction of a mm/hr) but potentially slower than those observed in switchgrass by Mann *et al.* [30], likely owing to the constrained geometry of the rhizobox in which our plants were grown (in comparison to field grown plants). The average growth rate of the main root was 0.08 ± 0.03 mm/hr. The average growth rates of the two measured root hairs were both 0.07 ± 0.02 mm/hr. Linear trend lines in Fig. 7(A) show that the growth rate appears to be declining for all three roots over the observed period. Root growth rates are known to respond to environmental conditions, and diurnal cycling or slight changes in conditions may have initiated the observed shift.

The above figures demonstrate OCT applicability to observing plant roots in soil. OCT is also suitable for imaging other parts of the plant [18–22]. Figure 8 and Vis. 6 show images of switchgrass stem, leaf, and seeds. The images can show the surface layer and a few subsurface layers of cells in the plant stem

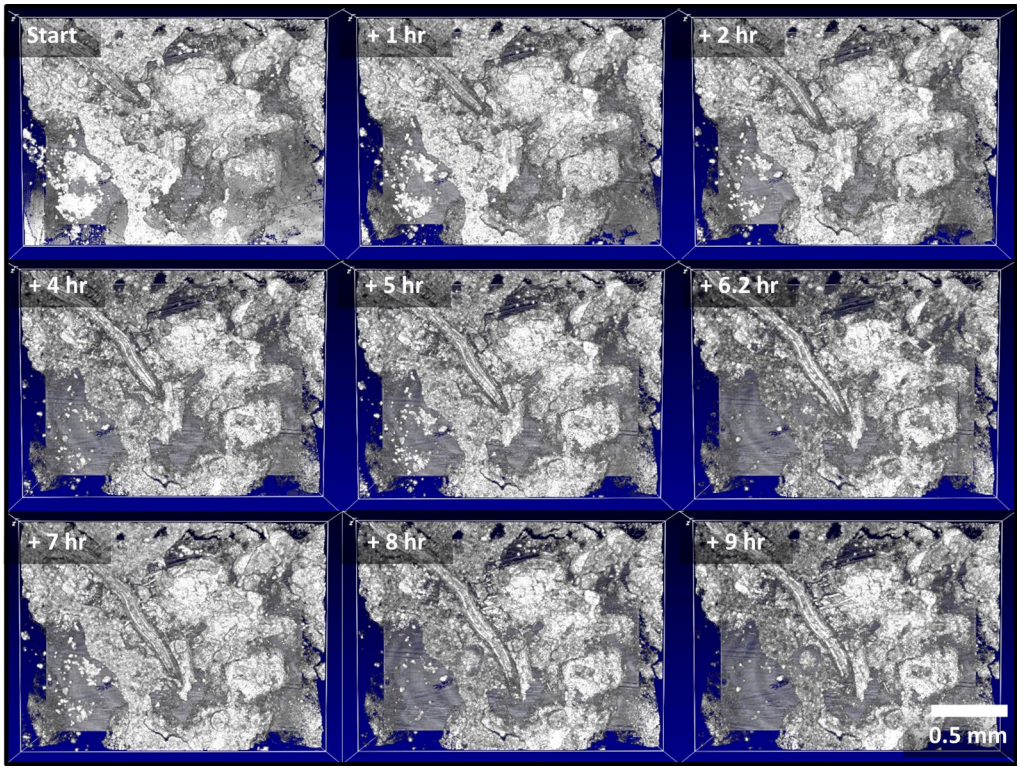

Fig. 6. Series of OCT images showing switchgrass root growth over 9 hrs. Scale is shown at lower right.

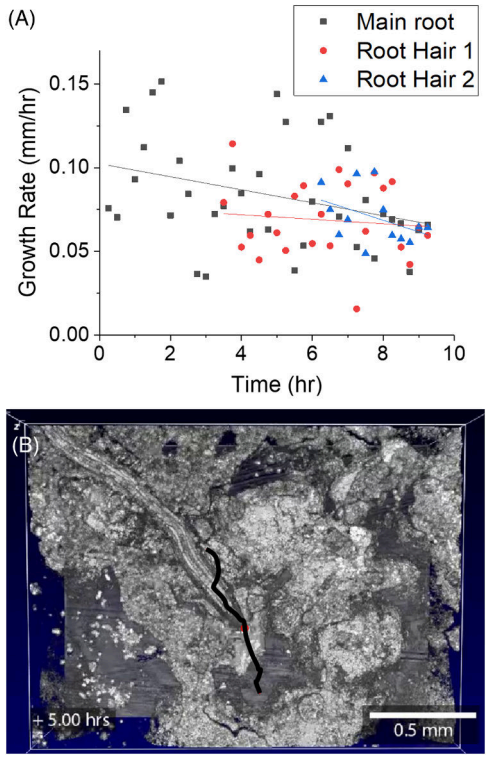

Fig. 7. (A) Plot of growth rates from the primary root (black square) and two root hairs (orange dot and blue triangle) as measured from the images shown in Fig. 6 and Visualization 4. Linear trend lines for each series are shown in the corresponding color. (B) An image midway through the observed time period with a trace of the path of the root tip shown in black.

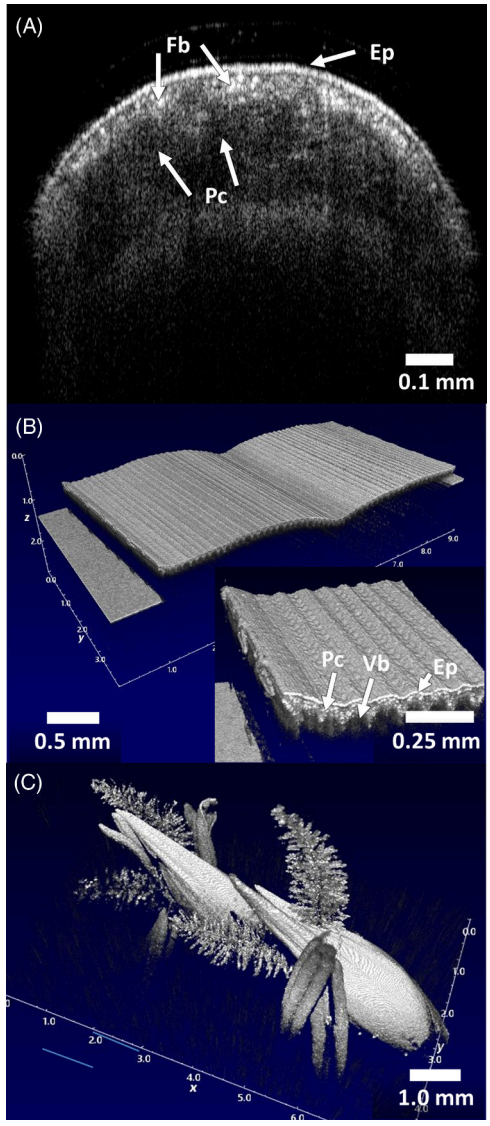

Fig. 8. (A) OCT cross section of a switchgrass stem with labels for the epidermis (Ep), fiber bundles (Fb), and parenchyma cells (Pc). (B) 3D surface image of switchgrass leaf with a magnified inset of the leaf's edge. The magnified inset has labels for the epidermis (Ep), parenchyma cells (Pc), and vascular bundles (Vb). (C) 3D image of a group of switchgrass seeds with the stamen and stigma. Scales are indicated by a bar in each image.

and leaf tissues. The stem and leaf cross sections clearly show the epidermal cells (Ep). Fiber bundles (Fb), vascular bundles (Vb), and parenchyma cells (Pc) are noticeably less defined, especially as the depth below the surface of the plant increases. Notably, Fig. 8C shows the plant's stamen and stigma extending from the seed pod floret. The pollen-producing stamen appears as a grouping of linear filaments. Four feather-like plumed stigma are visible in this image, and it is possible to distinguish each of the fine hairs of stigma within the focal range of the microscope. The rightmost stigma has clear details since it is better focused than the leftmost stigma, which likely fell below the optimal focal plane. Imaging of stomata on the leaf was attempted but not clearly resolved with the available imaging system. Future work focused on stomata imaging would require either a higher-resolution lens or to focus on plants with larger stomata. These images, along with root system images, demonstrate how OCT imaging can contribute to holistic observation of a developing plant. A challenge of analyzing time series OCT data is that current OCT analysis software does not have the capability to merge and align data from multiple time points. The images and video visualizations presented in this manuscript were constructed from static 2D captures of the 3D data. It would be more interesting and informative to align and integrate 3D time series data so it can be visually explored.

4. CONCLUSION

This work presented a new method of imaging plant roots in the challenging conditions of natural soil. The 3D images of roots may help to elucidate their interaction with heterogeneously distributed nutrients and other organisms in the soil. Growing the plants in an angled rhizobox with a thick imaging window facilitated OCT root imaging by ensuring growth against the surface of the window. OCT imaging with other rhizobox configurations may be possible, but it is likely that fewer roots will be optimally placed. The key advantages of OCT imaging are (1) a unique combination of lateral resolution and imaging depth, (2) non-destructive incident light that does not require use of contrast agents, and (3) relatively fast data acquisition in

a compact benchtop system. The key limitations include the shadow effect, where features become hidden below thick or opaque surface features and distortion that can result from a lens effect in the first layer of cells. A requirement for a long-term time series is a computer with enough memory to store many multi-gigabyte files. We found that the memory available on our system limited either the imaging interval or the recording period, and the system had to be reset for long data-collection periods. OCT can become a valuable tool for a variety of plant studies. For instance, the non-destructive nature of OCT can be leveraged to help elucidate morphological root responses to environmental perturbations, including those associated with desiccation stress, pathogen exposure, competition between neighboring plants, or bioturbation by various macrofauna. The high spatial resolution of OCT will also permit analysis of the fine-scale interactions between roots and soil microbial hotspots or associations with fungi or bacteria-induced nodules. Finally, we reiterate that OCT is completely non-destructive and does not require any addition of contrasting agents or other exogenous material. Thus, OCT may be employed as a preliminary screening technique whereby the resulting highly resolved images can be used to direct the timing or spatial location of sample collection for a suite of omics, culturing, or further refined imaging techniques.

Funding. Office of Science (Early Career Research Program); Laboratory Directed Research and Development (DE-AC05-7601830).

Acknowledgment. We acknowledge Vivian Lin for help with plant growth. We thank three anonymous reviewers for their helpful comments. Support for this research was provided by the Great Lakes Bioenergy Research Center, U.S. Department of Energy, Office of Science, Office of Biological and Environmental Research (Awards DE-SC0018409 and DE-FC02-07ER64494), by the National Science Foundation Long-term Ecological Research Program (DEB 1637653) at the Kellogg Biological Station, and by Michigan State University AgBioResearch.

Disclosures. The authors declare that there are no conflicts of interest related to this paper.

REFERENCES

1. I. M. Young and J. W. Crawford, "Interactions and self-organization in the soil-microbe complex," Science **304**, 1634–1637 (2004).
2. A. Hodge, "The plastic plant: root responses to heterogeneous supplies of nutrients," New Phytol. **162**, 9–24 (2004).
3. M. Holz, M. Zarebanadkouki, Y. Kuzyakov, J. Pausch, and A. Carminati, "Root hairs increase rhizosphere extension and carbon input to soil," Ann. Bot. **121**, 61–69 (2018).
4. C. Kaiser, M. R. Kilburn, P. L. Clode, L. Fuchslueger, M. Koranda, J. B. Cliff, Z. M. Solaiman, and D. V. Murphy, "Exploring the transfer of recent plant photosynthates to soil microbes: mycorrhizal pathway vs direct root exudation," New Phytol. **205**, 1537–1551 (2015).
5. H. Marschner and B. Dell, "Nutrient uptake in mycorrhizal symbiosis," Plant Soil **159**, 89–102 (1994).
6. A. H. Ahkami, R. A. White, III, P. P. Handakumbura, and C. Jansson, "Rhizosphere engineering: enhancing sustainable plant ecosystem productivity," Rhizosphere **3**, 233–243 (2017).
7. D. L. Jones, C. Nguyen, and R. D. Finlay, "Carbon flow in the rhizosphere: carbon trading at the soil–root interface," Plant Soil **321**, 5–33 (2009).
8. J. Zhu, P. A. Ingram, P. N. Benfey, and T. Elich, "From lab to field, new approaches to phenotyping root system architecture," Curr. Opin. Plant Biol. **14**, 310–317 (2011).
9. S. J. Mooney, T. P. Pridmore, J. Helliwell, and M. J. Bennett, "Developing x-ray computed tomography to non-invasively image 3-D root systems architecture in soil," Plant Soil **352**, 1–22 (2012).
10. E. Oburger and H. Schmidt, "New methods to unravel rhizosphere processes," Trends Plant Sci. **21**, 243–255 (2016).
11. L. Li, Q. Zhang, and D. Huang, "A review of imaging techniques for plant phenotyping," Sensors **14**, 20078–20111 (2014).
12. J. Welzel, "Optical coherence tomography in dermatology: a review," Skin Res. Technol. **7**, 1–9 (2001).
13. J. M. Schmitt, "Optical coherence tomography (OCT): a review," IEEE J. Sel. Top. Quantum Electron. **5**, 1205–1215 (1999).
14. A. M. Zysk, F. T. Nguyen, A. L. Oldenburg, D. L. Marks, and S. A. Boppart, "Optical coherence tomography: a review of clinical development from bench to bedside," J. Biomed. Opt. **12**, 051403 (2007).
15. U. Sharma, N. M. Fried, and J. U. Kang, "All-fiber common-path optical coherence tomography: sensitivity optimization and system analysis," IEEE J. Sel. Top. Quantum Electron. **11**, 799–805 (2005).
16. K. Shen, H. Lu, S. Baig, and M. R. Wang, "Improving lateral resolution and image quality of optical coherence tomography by the multi-frame superresolution technique for 3D tissue imaging," Biomed. Opt. Express **8**, 4887–4918 (2017).
17. N. K. Ravichandran, R. E. Wijesinghe, M. F. Shirazi, K. Park, S.-Y. Lee, H.-Y. Jung, M. Jeon, and J. Kim, "In vivo monitoring on growth and spread of gray leaf spot disease in capsicum annuum leaf using spectral domain optical coherence tomography," J. Spectrosc. **2016**, 1–6 (2016).
18. R. E. Wijesinghe, S.-Y. Lee, N. K. Ravichandran, S. Han, H. Jeong, Y. Han, H.-Y. Jung, P. Kim, M. Jeon, and J. Kim, "Optical coherence tomography-integrated, wearable (backpack-type), compact diagnostic imaging modality for in situ leaf quality assessment," Appl. Opt. **56**, D108–D114 (2017).
19. J. C. Clements, A. V. Zvyagin, K. K. M. B. D. Silva, T. Wanner, D. D. Sampson, and W. A. Cowling, "Optical coherence tomography as a novel tool for non-destructive measurement of the hull thickness of lupin seeds," Plant Breeding **123**, 266–270 (2004).
20. A. Reeves, R. L. Parsons, J. W. Hettinger, and J. I. Medford, "In vivo three-dimensional imaging of plants with optical coherence microscopy," J. Microsc. **208**, 177–189 (2002).
21. I. V. Meglinski, C. Buranachai, and L. A. Terry, "Plant photonics: application of optical coherence tomography to monitor defects and rots in onion," Laser Phys. Lett. **7**, 307 (2010).
22. L. K. T. Srimal, U. M. Rajagopalan, and H. Kadono, "Functional optical coherence tomography (fOCT) biospeckle imaging to investigate response of plant leaves to ultra-short term exposure of Ozone," J. Phys.: Conf. Ser. **605**, 1–10 (2015).
23. V. V. Sapozhnikova, V. A. Kamensky, R. V. Kuranov, I. Kutis, L. B. Snopova, and A. V. Myakov, "In vivo visualization of Tradescantia leaf tissue and monitoring the physiological and morphological states under different water supply conditions using optical coherence tomography," Planta **219**, 601–609 (2004).
24. T. H. Chow, K. M. Tan, B. K. Ng, S. G. Razul, C. M. Tay, T. F. Chia, and W. T. Poh, "Diagnosis of virus infection in orchid plants with high-resolution optical coherence tomography," J. Biomed. Opt. **14**, 014006 (2009).
25. J. Sharpe, U. Ahlgren, P. Perry, B. Hill, A. Ross, J. Hecksher-Sorensen, R. Baldock, and D. Davidson, "Optical projection tomography as a tool for 3D microscopy and gene expression studies," Science **296**, 541–545 (2002).
26. K. J. I. Lee, G. M. Calder, C. R. Hindle, J. L. Newman, S. N. Robinson, J. Avondo, and E. S. Coen, "Macro optical projection tomography for large scale 3D imaging of plant structures and gene activity," J. Exp. Bot. **68**, 527–538 (2017).
27. J. Rueckel, M. Stockmar, F. Pfeiffer, and J. Herzen, "Spatial resolution characterization of a X-ray microCT system," Appl. Radiat. Isot. **94**, 230–234 (2014).

28. S. Schlüter, F. Leuther, S. Vogler, and H. J. Vogel, "X-ray microtomography analysis of soil structure deformation caused by centrifugation," Solid Earth **7**, 129–140 (2016).
29. D. van Dusschoten, R. Metzner, J. Kochs, J. A. Postma, D. Pflugfelder, J. Buhler, U. Schurr, and S. Jahnke, "Quantitative 3D analysis of plant roots growing in soil using magnetic resonance imaging," Plant Physiol. **170**, 1176–1188 (2016).
30. J. J. Mann, J. N. Barney, G. B. Kyser, and J. M. DiTomaso, "Root system dynamics of Miscanthus x giganteus and Panicum virgatum in response to rainfed and irrigated conditions in California," Bioenerg. Res. **6**, 678–687 (2013).

Query

1. AU: The funding information for this article has been generated using the information you provided to OSA at the time of article submission. Please check it carefully. If any information needs to be corrected or added, please provide the full name of the funding organization/institution as provided in the CrossRef Open Funder Registry (https://search.crossref.org/funding).